# Structures and luminescence properties of $Yb^{3+}$ in the double perovskites $Ba_2YB'O_6$ ($B'$=$Ta^{5+}$, $Nb^{5+}$) phosphors*

Zhou Wen-Long(周文龙)[a)b)], Zhang Qing-Li(张庆礼)[a)†], Gao Jin-Yun(高进云)[a)b)], Liu Wen-Peng(刘文鹏)[a)], Ding Li-Hua(丁丽华)[a)b)], and Yin Shao-Tang(殷绍唐)[a)]

[a)] *Anhui Provincial Key Laboratory of Photonic Devices and Materials, Anhui Institute of Optics and Fine Mechanics, Chinese Academy of Sciences, Hefei* 230031, *China*

[b)] *Graduate School of the Chinese Academy of Sciences, Beijing* 100049, *China*

(Received 5 June 2010; revised manuscript received 28 July 2010)

The $Yb^{3+}$ doped $Ba_2YB'O_6$ ($B'$=$Ta^{5+}$, $Nb^{5+}$) were prepared by high temperature solid-state reaction method, their structures were determined by x-ray diffraction and refined by Rietveld method. The diffuse reflection absorption, excitation and emission spectra of $Yb^{3+}$:$Ba_2YB'O_6$ ($B'$=$Ta^{5+}$, $Nb^{5+}$) were measured at room temperature. Under the excitation of ultraviolet light, these phosphors exhibit broad charge transfer band emissions of $TaO_6$ or $NbO_6$ centre with large Stokes shift. The $Yb^{3+}$ doped into these hosts are situated at $Y^{3+}$ sites of cubic symmetry ($O_h$). The experimental energy levels of $Yb^{3+}$ in $Ba_2YTaO_6$ and $Ba_2YNbO_6$ were determined by photoluminescence and diffuse reflection absorption spectra. Their wavefunctions and theoretical energy levels were obtained by diagonalising the Hamiltonian matrix. The experimental energy levels were fitted by Levenberg–Marquardt iteration algorithm to determine crystal field parameters. Then, the magnetic-pole transition line strengths of $Yb^{3+}$:$Ba_2YB'O_6$ ($B'$=$Ta^{5+}$, $Nb^{5+}$) from $(^2F_{5/2})\Gamma_8^-$ to the low-energy states were calculated.

**Keywords:** luminescence properties, $Yb^{3+}$, $Ba_2YTaO_6$, $Ba_2YNbO_6$
**PACS:** 61.10.Nz, 71.70.Ch, 78.55.–m, 75.10.Dg **DOI:** 10.1088/1674-1056/20/1/016101

## 1. Introduction

Double perovskite-type oxides have the formula $A_2BB'O_6$, in which $A$ represents a large cation and $B$ (or $B'$) represents a small cation. The ideal perovskite structure is composed of a three-dimensional framework of corner-sharing $BO_6$ and $B'O_6$ octahedra, alternately. This framework forms cube-octahedral cavities which are filled by $A$-site cations. Recently, emerging interest is focused on double perovskite-type oxides, which is the result of the variety of interesting properties of these compounds due to their compositional and structural diversity. Some of them have been applied in a number of fields such as substrates for high $T_c$ superconductors,[1] electrode materials for solid state fuel cells,[2] dielectric resonators,[3] promising materials used as host for phosphors[4,5] and so on.

$Yb^{3+}$ doped phosphor with high symmetry can be used as the laser medium, because of its advantage to avoid cracking induced by the thermal stress from thermal load during laser operation or temperature gradient during crystal growth. $Yb^{3+}$ has only two multiplets $^2F_{7/2}$ and $^2F_{5/2}$ without deleterious upconversion and cross-relaxation. Meanwhile, its quantum defect is low and energy lifetime is long which result in low thermal load and good energy storage ability, and its wide absorption band is very promising for laser-diode pump. A considerable amount of experimental and theoretical works have been done on the $Yb^{3+}$ ions in sites of cubic symmetry in the perovskite-type crystals such as $A_2BLnF_6$[6] and $ABF_3$.[7,8] Those results demonstrate unambiguously that the crystal field on $Yb^{3+}$ ions in cubic symmetry ($O_h$) site is extremely strong. $Ba_2YTaO_6$ and $Ba_2YNbO_6$ are cubic system crystals with the space group $Fm\bar{3}m$ at room temperature.[9,10] The $Y^{3+}$ and $Ta^{5+}$/$Nb^{5+}$ ions are arranged respectively at the centres of $YO_6$ and $TaO_6$/$NbO_6$ octahedra. To the best of our knowledge, it is the first time to investigate the structures, photoluminescence and crystal field splitting of the $Yb^{3+}$-doped double perovskite-type oxides $Ba_2YB'O_6$

*Project supported by the National Natural Science Foundation of China (Grant Nos. 50772112, 90922003, and 50872135), Provincial Natural Science Fund of Anhui, China (Grant No. 08040106820), and the Knowledge Innovation Program of the Chinese Academy of Sciences (Grant No. YYYJ-1002).

†Corresponding author. E-mail: zql@aiofm.ac.cn

© 2011 Chinese Physical Society and IOP Publishing Ltd

($B'$= $Ta^{5+}$, $Nb^{5+}$) presented in this paper.

## 2. Experimental

The phosphor samples $Yb^{3+}$:$Ba_2YB'O_6$ ($B'$= $Ta^{5+}$, $Nb^{5+}$) were synthesised by high temperature solid state reaction method. The starting materials were $Ba(NO_3)_2$, $Y_2O_3$, $Ta_2O_5$(or $Nb_2O_5$) and $Yb_2O_3$ (with 99.99% purity). The doping concentrations of $Yb^{3+}$ ions were 5 at.% in $Ba_2YB'O_6$ ($B'$= $Ta^{5+}$, $Nb^{5+}$) hosts. Stoichiometric amounts of $Ba(NO_3)_2$, $Y_2O_3$, $Ta_2O_5$(or $Nb_2O_5$), $Yb_2O_3$ were thoroughly mixed and ground using an agate mortar and pestle. In order to get a well-crystalline phase, the mixtures were preheated in air at 800 °C for 12 h to decompose $Ba(NO_3)_2$. After that, the products were reground and heated by a medium frequency induction furnace. The samples were sintered at 1600 °C for 72 h then naturally cooled to room temperature and grind carefully as the final samples.

The structures of 5 at.% $Yb^{3+}$:$Ba_2Y_{0.95}B'O_6$ ($B'$= $Ta^{5+}$, $Nb^{5+}$) were determinated by x-ray diffraction (XRD). The XRD patterns were recorded by Philips X'pert PRO x-ray diffractometer with $CuK_\alpha$ radiation ($\lambda$ = 0.15405 nm) operated at 40 kV and 40 mA, and the scan step of $2\theta$ was 0.033492° in the range of 20°–80°. Excitation and emission spectra were measured by a Fluorolog-3-Tan spectrometer. Diffuse reflection absorption spectra were measured by a Japanese Shimadzu Solid Spec-3700 DUV-UV-Visible-Near Infrared spectrophotometer. All the measurements were carried out at room temperature.

## 3. Results and discussion

### 3.1. Structures of 5 at.% $Yb^{3+}$:$Ba_2Y_{0.95}B'O_6$ ($B'$= $Ta^{5+}$, $Nb^{5+}$)

Figures 1 and 2 show the x-ray powder diffraction patterns of the 5 at.% $Yb^{3+}$:$Ba_2Y_{0.95}B'O_6$ ($B'$= $Ta^{5+}$, $Nb^{5+}$), which are consistent with their standard powder diffraction files (JCPDS files: 19-147, 24-1042). No other phases are detected. The 5 at.% $Yb^{3+}$:$Ba_2Y_{0.95}B'O_6$ crystal structures were refined by Rietveld method[11] with the general structure analysis system software (GSAS).[12] The atomic fractional coordinates of $Ba_2YTaO_6$ were used as the refinement initial values.[13] The residuals $R_p$ and $R_{wp}$ of $Ba_2Yb_{0.05}Y_{0.95}TaO_6$, $Ba_2Yb_{0.05}Y_{0.95}NbO_6$ were 6.04%, 7.65%, and 6.13%, 7.87%, respectively. These values are very small, indicating that the fitted and experimental curves are consistent very well. The fitted structure parameters by Rietveld method are listed in Table 1 and the x-ray diffraction index $HKL$ have been shown in Figs. 1 and 2.

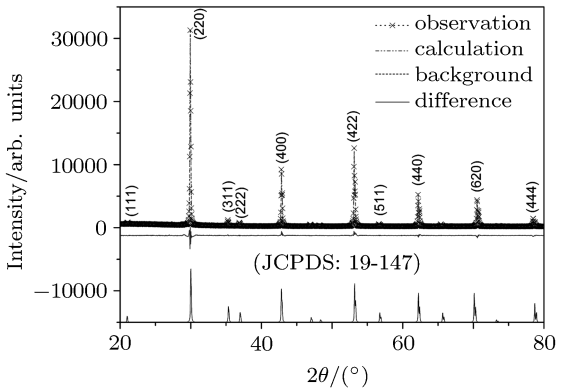



**Fig. 1.** X-ray powder diffraction patterns and Rietveld fitting curves of 5 at.% $Yb^{3+}$:$Ba_2Y_{0.95}TaO_6$ polycrystalline material.

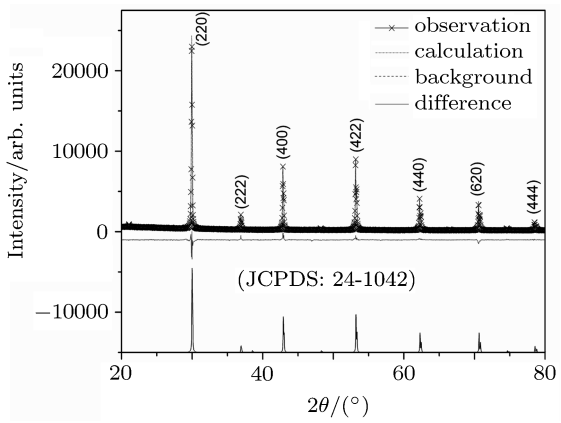



**Fig. 2.** X-ray powder diffraction patterns and Rietveld fitting curves of 5 at.% $Yb^{3+}$:$Ba_2Y_{0.95}NbO_6$ polycrystalline material.

Figure 3 exhibits the crystal structure of $Ba_2YTaO_6$, which belongs to the cubic crystal system with the $Fm\bar{3}m$ space group, and there are four $Ba_2YTaO_6$ formulas in a unit cell ($Z = 4$). The structure of $Ba_2YNbO_6$ is similar to that of $Ba_2YTaO_6$. The unit cell of $Ba_2YTaO_6$ is a cube divided into eight small cubes. In the small cubes, the $Ba^{2+}$ions are positioned at the corners, the $O^{2-}$ ions are positioned at the middle of the sides and the alternating $Y^{3+}$ and $Nb^{5+}$ (or $Ta^{5+}$) ions are positioned in the centre. This space group allows two crystallographically distinct octahedral sites in the perovskite structure, thus permitting 1:1 positional ordering between the $Y^{3+}$ and $Ta^{5+}$ (or $Nb^{5+}$) ions. The appearance of superlattice lines (111), (311) and (511) confirm that the salt-rock type ordering of $Y^{3+}$ and $Ta^{5+}$ (Fig. 1). But these lines are too weak to be detected in 5 at.% $Yb^{3+}$:$Ba_2Y_{0.95}NbO_6$ (Fig. 2).

**Table 1.** Summary of the Rietveld's structural refinement to $Ba_2Yb_{0.05}Y_{0.95}TaO_6$ and $Ba_2Yb_{0.05}Y_{0.95}NbO_6$ crystals. (1 Å=0.1 nm)

| $Ba_2\ Yb_{0.05}\ Y_{0.95}TaO_6$ | | | | | | $Ba_2Yb_{0.05}Y_{0.95}NbO_6$ | | | | | |
|---|---|---|---|---|---|---|---|---|---|---|---|
| | | $X$ | $Y$ | $Z$ | Uiso*/Å$^2$ | | | $X$ | $Y$ | $Z$ | Uiso*/Å$^2$ |
| $Ba^{2+}$ | 8c | 0.25 | 0.25 | 0.25 | 0.0065 | $Ba^{2+}$ | 8c | 0.25 | 0.25 | 0.25 | 0.0099 |
| $Y^{3+}$ | 4a | 0 | 0 | 0 | 0.0039 | $Y^{3+}$ | 4a | 0 | 0 | 0 | 0.008 |
| $Yb^{3+}$ | 4a | 0 | 0 | 0 | 0.0039 | $Yb^{3+}$ | 4a | 0 | 0 | 0 | 0.008 |
| $Ta^{5+}$ | 4b | 0.5 | 0.5 | 0.5 | 0.0021 | $Nb^{5+}$ | 4b | 0.5 | 0.5 | 0.5 | 0.001 |
| $O^{2-}$ | 24e | 0.25698 | 0 | 0 | 0.0135 | $O^{2-}$ | 24e | 0.26415 | 0 | 0 | 0.03 |
| $a=b=c$/Å | | | $\beta$ | $V$/Å$^3$ | $\rho$/g·cm$^{-3}$ | $a=b=c$/Å | | | $\beta$ | $V$/Å$^3$ | $\rho$/g·cm$^{-3}$ |
| 8.43712 | | | 90° | 600.595 | 7.130 | 8.43579 | | | 90° | 600.313 | 6.159 |
| $R_p^{**}=6.04\%$ | | | | | | $R_p^{**}=6.13\%$ | | | | | |
| $R_{wp}^{***}=7.65\%$ | | | | | | $R_{wp}^{***}=7.87\%$ | | | | | |

*: Constraint on isotropic atomic displacement factor of Uiso($Y^{3+}$)=Uiso($Yb^{3+}$) was used. **: $R_p=\sum|F_{exp}-F_{cacl}|/\sum|F_{exp}|$. ***: $R_{wp}=\left[\sum w_i\left(F_{exp}-F_{cacl}\right)^2/\sum w_i\left(F_{exp}\right)^2\right]^{1/2}$.

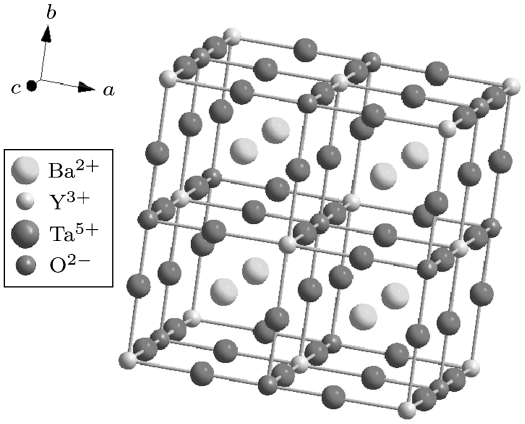



**Fig. 3.** Crystal structure of the double perovskite $Ba_2YTaO_6$.

On the basis of the results of luminescence measurements, Yu *et al.*[5] concluded that the $Eu^{3+}$ ions occupy the $Gd^{3+}$sites with cubic inversion symmetry ($O_h$) in the $Ba_2GdNbO_6$ host. Obviously, the doped $Yb^{3+}$ ions prefer to occupy the $Y^{3+}$ sites with high symmetry ($O_h$), based on their close ionic radii [$r$ ($Yb^{3+}$)=1.008 Å, $r$ ($Y^{3+}$)=1.04 Å] and identical valence state (+3) in $Ba_2YB'O_6$. During our refinement, $Yb^{3+}$ was placed in the $Y^{3+}$ site which seems reasonable due to good consistence between the calculated and experimental curves of XRD. So the doped $Yb^{3+}$ ions possess cubic inversion symmetry ($O_h$) in $Ba_2YB'O_6$ hosts.

The strengths of crystal-field can be predicted by some physical parameters such as coordination, bond length and bond angle. These parameters are calculated and listed in Table 2.

**Table 2.** Atom sites and bond lengths in $Ba_2YTaO_6$ and $Ba_2YNbO_6$ ($Ln^{3+}=Y^{3+}$, $Yb^{3+}$; $M^{5+}=Ta^{5+}$, $Nb^{5+}$).

| host | $Ln^{3+}$, $M^{5+}$ sites | | $Ln^{3+}$–$O^{2-}$/Å | $M^{5+}$–$O^{2-}$/Å | $M^{5+}$–$O^{2-}$–$M^{5+}$/(°) |
|---|---|---|---|---|---|
| | symmetry | coordination | | | |
| $Ba_2YTaO_6$ | $O_h$ | 6 | 2.168 | 2.05 | 180° |
| $Ba_2YNbO_6$ | $O_h$ | 6 | 2.228 | 1.99 | 180° |

## 3.2. Luminescence of 5 at.% $Yb^{3+}$:$Ba_2Y_{0.95}B'O_6$ ($B'$= $Ta^{5+}$, $Nb^{5+}$)

The excitation and emission spectra of 5 at.% $Yb^{3+}$:$Ba_2Y_{0.95}TaO_6$ and 5 at.% $Yb^{3+}$:$Ba_2Y_{0.95}NbO_6$ in the ultraviolet and visible spectral region at room temperature are shown in Figs. 4 and 5, respectively, which are wide spectral bands. The strongest excitation peaks of $Yb^{3+}$:$Ba_2YTaO_6$ and $Yb^{3+}$:$Ba_2YNbO_6$ locate at 263 and 314 nm, with emission maximum peaks at 390 and 530 nm, respectively. Compared with the spectra of $Yb^{3+}$:$Ba_2YTaO_6$, the spectra of $Yb^{3+}$:$Ba_2YNbO_6$ show larger red shift. Eng *et al.*[14] have studied the relationships among composition, crystal structure and the electronic structure of oxides containing octahedrally coordinated $d^0$ transition metal ions The ions investigated in Ref. [14] ($Ti^{4+}$, $Nb^{5+}$, $Ta^{5+}$, $Mo^{6+}$, and $W^{6+}$) were focused

primarily on perovskite and perovskite-related structures. In these compounds, the top of the valence band (VB) is primarily composed of oxygen 2p nonbonding, while the conduction band (CB) arises from the $\pi^*$ interaction between the transition metal $t_{2g}$ orbitals and oxygen. The transition from VB to CB can be described as an oxygen-to-metal charge transfer excitation. For $Yb^{3+}$:$Ba_2YTaO_6$, the excitation band peak around 263 nm (Fig. 4), matching well with the band gap of $Ba_2YTaO_6$ (4.6 eV),[14] is assigned to the oxygen-to-tantalum charge transfer of the $TaO_6$ centre. The similar transfer occurs in $Yb^{3+}$:$Ba_2YNbO_6$. The electronegativity effect of $Nb^{5+}$ is larger than that of $Ta^{5+}$, which leads to the band gap of $Ba_2YNbO_6$ ($E_g \sim 3.8$ eV) lower than that of $Ba_2YTaO_6$ ($E_g \sim 4.6$ eV), as a result, the excitation band peak of $Yb^{3+}$:$Ba_2YNbO_6$ shifts to longer wavelength than that of $Yb^{3+}$:$Ba_2YTaO_6$, as shown in Fig. 5.

Complexes of transition metal ions with a formally empty $d$ shell such as $NbO_6$, $WO_6$[15] and $TaO_6$[16]often show intense broad-band emission with a large Stokes shift. In the present work, the emission bands of $Yb^{3+}$:$Ba_2YTaO_6$, $Yb^{3+}$:$Ba_2YNbO_6$ peaked at 390 and 530 nm, respectively (Figs. 4 and 5). The charge transfer luminescence of $Yb^{3+}$ ions are quenched at room temperature in the various host lattices,[17] so the emission bands are mainly caused by the charge transfer luminescence of $TaO_6$ and $NbO_6$ centres. The Stokes shifts between the maximum of the excitation band and that of the emission band are 12382 and 12979 $cm^{-1}$, respectively. The diffuse reflection absorption (DRS), excitation and emission spectra of 5 at.% $Yb^{3+}$:$Ba_2Y_{0.95}TaO_6$ phosphor in the near infrared region (NIR) is presented in Fig. 6, both of them have the same peak of 968 nm, which should belong to the

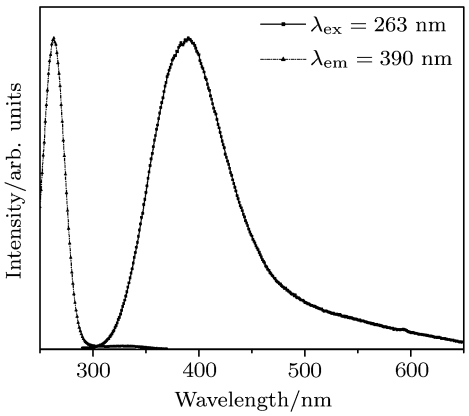



**Fig. 4.** Excitation and emission spectra of 5 at.% $Yb^{3+}$:$Ba_2Y_{0.95}TaO_6$ phosphor in the ultraviolet and visible spectral region at room temperature. Spectra are normalised at 263, 390 nm, respectively.

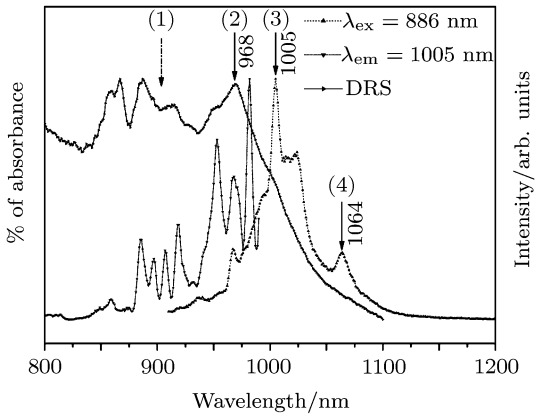



**Fig. 6.** The DRS, excitation and emission spectra of 5 at.% $Yb^{3+}$:$Ba_2Y_{0.95}TaO_6$ phosphor in the NIR region at room temperature. Spectra are normalised at 887, 982 and 1005 nm, respectively.

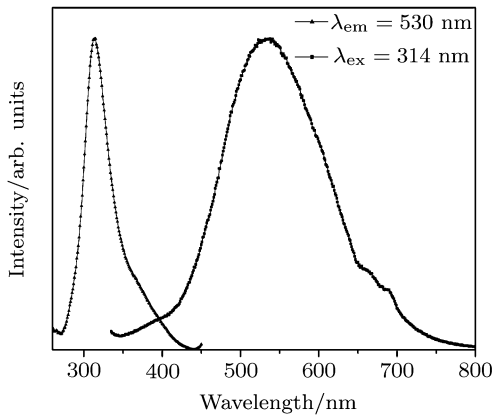



**Fig. 5.** Excitation and emission spectra of 5 at.% $Yb^{3+}$:$Ba_2Y_{0.95}NbO_6$ phosphor in the ultraviolet and visible spectral region at room temperature. Spectra are normalised at 314, 530 nm, respectively.

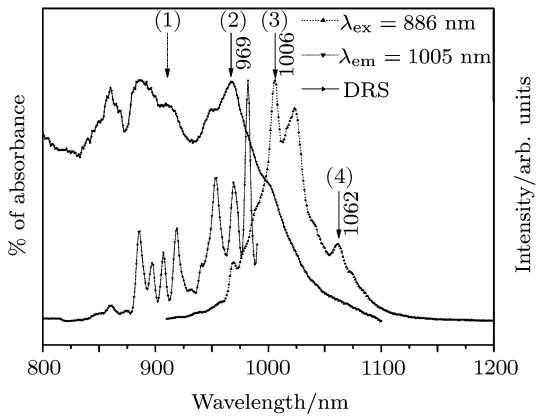



**Fig. 7.** The DRS, excitation and emission spectra of 5 at.% $Yb^{3+}$:$Ba_2Y_{0.95}NbO_6$ phosphor in the NIR region at room temperature. Spectra are normalised at 887, 982 and 1006 nm, respectively.

zero-line transition from the lowest levels of $^2F_{5/2}$ manifolds to the lowest levels of $^2F_{7/2}$ manifold of $Yb^{3+}$. The broad emission curve from 950 nm to 1100 nm mainly includes three bands around 968, 1005 and 1064 nm upon excitation by 886 nm. The emission band around 1064 nm is due to the transition from the lowest levels of $^2F_{5/2}$ manifold to the highest levels of $^2F_{7/2}$ manifold. The strongest broad band at 1005 nm is attributed to the electron transitions from the lowest levels of $^2F_{5/2}$ manifold to the sublevels of the $^2F_{7/2}$ multiplet. The low intensities of the shoulder-peaks and the large line-widths may be considered as electron-vibrational ones of purely electronic transitions. The coordination environment of the $Yb^{3+}$ ions in $Ba_2YNbO_6$ is similar to that of $Yb^{3+}$ ions in $Ba_2YTaO_6$ crystal and the distance between the $Yb^{3+}$ ions and the nearest ligands ions in both crystals are close to each other (Table 2). As expected, the optical spectra of $Yb^{3+}$ in $Ba_2YTaO_6$ and $Ba_2YNbO_6$ are similar, as shown in Figs. 6 and 7, where arrows labeled 1, 2, 3, 4 point out the spectral lines supposedly corresponding to the stark levels transitions of $Yb^{3+}$ ($O_h$), as shown in Figs. 8 and 9.

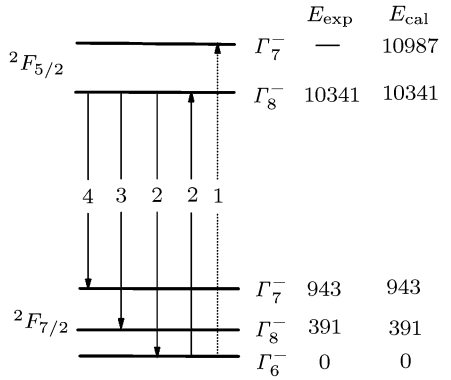



**Fig. 8.** The energy level structure of $Yb^{3+}$ in $Ba_2YTaO_6$.

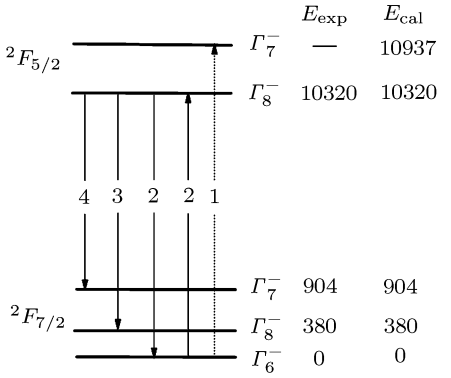



**Fig. 9.** The energy level structure of $Yb^{3+}$ in $Ba_2YNbO_6$.

### 3.3. Energy fitting of $Yb^{3+}$:$Ba_2Y_{0.95}B'O_6$ ($B'$= $Ta^{5+}$, $Nb^{5+}$)

Due to the high site symmetry of $Yb^{3+}$ in $Ba_2YTaO_6$ and $Ba_2YNbO_6$, it is possible to determine their crystal field Hamiltonian parameters by their experimental energy levels splitting. The parameterised Hamiltonian can be expressed as

$$H = H_{SO} + H_{CF} = \xi S \cdot L + \sum_{k,q} B_q^k C_q^k, \qquad (1)$$

where $\xi$ is spin-orbital interaction parameter, $S$ and $L$ are spin and orbital angular moment operators, respectively, $B_q^k$ is the crystal field parameter,$C_q^k$ is the angular operator. The crystal field Hamiltonian of $Yb^{3+}$ at site symmetry $O_h$ is simplified as[18]

$$\sum_{k,q} B_q^k C_q^k = B_0^4 \Big[ C_4^0 + \frac{\sqrt{5}}{\sqrt{14}}(C_{-4}^4 + C_4^4) + B_0^6 (C_6^0 - \frac{\sqrt{7}}{\sqrt{2}}(C_{-6}^6 + C_6^6)\Big], \qquad (2)$$

where, the independent parameters are $B_0^4$ and $B_0^6$, whose fourfold, threefold symmetry axes are [001] and [111] directions. The Hamiltonian matrix elements were calculated with the base vectors $\{|\boldsymbol{SLJM}\rangle\} = \{|^2F_{7/2},\ 7/2\rangle, \ldots,\ |^2F_{7/2},\ -7/2\rangle,\ |^2F_{5/2},\ 5/2\rangle, \ldots,\ |^2F_{5/2},\ -5/2\rangle\}$. The wavefunctions and theoretical energy levels were obtained by diagonalising the Hamiltonian matrix. The experimental energy levels were fitted by Levenberg–Marquardt iteration algorithm to determine Hamiltonian parameters $\xi$, $B_0^4$and $B_0^6$.[19,20] The fitting residual $R$ and root-mean-square $\sigma$ are defined as

$$R = \sqrt{\sum\nolimits_i (E_i^{exp} - E_i^{cal})^2 / \sum_i (E_i^{exp})^2}, \qquad (3)$$

$$\sigma = \sqrt{\sum\nolimits_i (E_i^{exp} - E_i^{cal})^2 / (N - N_{var})}, \qquad (4)$$

where $E_i^{exp}$ and $E_i^{cal}$ are experimental and calculated energy levels, respectively, $N$ is the energy level number, and $N_{var}$ is the fitted parameter number. $R$ and $\sigma$ can characterise the fitting effect, namely, consistency between experimental and calculated energy levels.

Both the initial fitting parameters of ($\xi$, $B_0^4$, $B_0^6$) for $Yb^{3+}$:$Ba_2YTaO_6$ and $Yb^{3+}$:$Ba_2YNbO_6$ are (2900, 600, 200). After twelve and eighteen iterations, the obtained values of ($\xi$, $B_0^4$, $B_0^6$) for $Yb^{3+}$:$Ba_2YTaO_6$ and $Yb^{3+}$:$Ba_2YNbO_6$ are (2889, 2263, 113), (2885, 2165, 122), with the results of $R$ and $\sigma$ being 0.0001% and 0.0082 $cm^{-1}$, 0.0001% and 0.0047 $cm^{-1}$, respectively.

The fitted results are shown in Table 3. It can be seen that the calculated energy values are consistent with the experimental values very well.

**Table 3.** Parameters $B_q^k$, $\xi$ and energy levels (in $cm^{-1}$) of $Yb^{3+}$ ($O_h$) in $Ba_2YTaO_6$ and $Ba_2YNbO_6$.

| $J$ | energy level | $Ba_2YTaO_6$ | | $Ba_2YNbO_6$ | |
|---|---|---|---|---|---|
| | | experiment | theory | experiment | theory |
| 5/2 | $\Gamma_7^-$ | – | 10987 | – | 10937 |
| | $\Gamma_8^-$ | 10341 | 10341 | 10320 | 10320 |
| 7/2 | $\Gamma_7^-$ | 943 | 943 | 904 | 904 |
| | $\Gamma_8^-$ | 391 | 391 | 380 | 380 |
| | $\Gamma_6^-$ | 0 | 0 | 0 | 0 |
| | $\xi$ | | 2889 | | 2885 |
| | $B_0^4$ | | 2263 | | 2165 |
| | $B_0^6$ | | 113 | | 122 |

The quadratic rotational invariants in terms of the crystal field parameters is defined as[21]

$$s_k^2 = \frac{1}{2k+1}\sum_{q=-k}^{k}|B_q^k|^2, \tag{5}$$

and the quadratic moments $(\sigma_2(\alpha SLJ))^2$of the multiplets $|\alpha SLJ\rangle$ can be expressed as

$$\begin{aligned}&(\sigma_2(\alpha SLJ))^2\\ &= \frac{1}{2J+1}\sum_{k=2,4,6} s_k^2\langle\alpha SLJ||C^{(k)}||aLSJ\rangle^2\\ &= \frac{1}{2J+1}\sum_i\left[E_i(\alpha SLJ)-E^0(\alpha SLJ)\right]^2,\end{aligned} \tag{6}$$

where $E^0(\alpha SLJ)$ is the mean energy. It is useful to use the crystal field parameters to predict the energy splitting magnitude $\Delta E(\alpha SLJ) = \sqrt{\sum_i\left[E_i(\alpha SLJ)-E^0(\alpha SLJ)\right]^2}$ of $Yb^{3+}$ for exploring the new $Yb^{3+}$ laser materials, which can characterise the crystal field energy splitting to some extent. The relation between the maximum crystal field splitting $\Delta E$ of a $^{2S+1}L_J$ multiplet and the scalar crystal field strength parameter $N_v$ is[22]

$$\Delta E = \left[\frac{3g_A^2}{g(g_A+2)(g_A+1)\pi}\right]^{1/2}\left[\prod_{k=2,4,6}|\langle aSLJ||U^{(k)}||aSLJ\rangle\langle 3||C^k||3\rangle|\right]^{1/3}N_v, \tag{7}$$

$$N_v = \left[\sum_{k,q}\frac{4\pi}{2k+1}(B_q^k)^2\right]^{1/2}, \tag{8}$$

where $g_A$ is the degeneracy effectively removed by the crystal field, $g$ is the total generacy of the $^{2S+1}L_J$ multiplet. $\Delta E$ may be labeled as $\Delta E'$ in order to distinguish it from the mentioned $\Delta E(\alpha SLJ)$ previously. All of these parameters are calculated and listed in Table 4.

**Table 4.** Quadratic rotational invariants and crystal field energy splittings of $Yb^{3+}$ in $Ba_2YTaO_6$ and $Ba_2YNbO_6$.

| | Yb:$Ba_2YTaO_6$ | Yb:$Ba_2YNbO_6$ |
|---|---|---|
| $S_k^2(k=2,4,6)/(cm^{-1})^2$ | 0, 975694, 7795 | 0, 892722, 9111 |
| $N_v$ | 3516 | 3366 |
| $(\sigma_2(^2F_{7/2}))^2/(cm^{-1})^2$ | 106849 | 97816 |
| $(\sigma_2(^2F_{5/2}))^2/(cm^{-1})^2$ | 53099 | 48584 |
| $\Delta E^{cal}(^2F_{7/2})/cm^{-1}$ | 924 | 884 |
| $\Delta E'^{cal}(^2F_{7/2})/cm^{-1}$ | 790 | 756 |
| $\Delta E^{exp}(^2F_{7/2})/cm^{-1}$ | 943 | 904 |
| $\Delta E^{cal}(^2F_{5/2})/cm^{-1}$ | 743 | 540 |
| $\Delta E'(^2F_{5/2})/cm^{-1}$ | / | / |
| $\Delta E^{exp}(^2F_{5/2})/cm^{-1}$ | $\sim 646$ | $\sim 617$ |

It can be seen that $S_2^2$ predominates the crystal field energy splitting, and the value of $Yb^{3+}$:$Ba_2YTaO_6$ is much more than that of $Yb^{3+}$:$Ba_2YNbO_6$, with the result that $\Delta E(\alpha SLJ)$ are more than that of $Yb^{3+}$:$Ba_2YNbO_6$, although $S_4^2$ is more than that of $Yb^{3+}$:$Ba_2YTaO_6$. On the other hand, it can be seen that the calculated root-mean-square difference $\Delta E^{cal}(\alpha SLJ)$is closer to the crystal field energy splitting maximum $\Delta E^{exp}(\alpha SLJ)$, which shows that it is useful to predict crystal energy splitting of magnetic ion in solids by the crystal field parameters and the quadratic moments $(\sigma_2(\alpha SLJ))^2$. The difference between $\Delta E'^{cal}(^2F_{7/2})$ and $\Delta E^{exp}(^2F_{7/2})$ for $^2F_{7/2}$ of $Yb^{3+}$:$Ba_2YTaO_6$ and $Yb^{3+}$:$Ba_2YNbO_6$ are as large as 153 and 148 $cm^{-1}$, respectively. On the other hand, in some cases $\langle aSLJ||U^{(k)}||aSLJ\rangle$ would be zero, and Eqs. (7) and (8) can not be used to predict crystal-field splitting. Here the value $\langle^2F_{5/2}||U^{(6)}||^2F_{5/2}\rangle$ is zero, so $\Delta E'(^2F_{5/2})$ can not be calculated. It seems that it is not very good to use Eqs. (7) and (8) to predict the maximum crystal-field splitting.

The wavefuctions of $Yb^{3+}$ in $Ba_2YTaO_6$ in energy ascending order are expressed as the following in the irreducible representations of $O_h$:

$\Psi_1$: $-|3.5, \Gamma_6^-_2\rangle$ (100%)

$\Psi_2$: $|3.5, \Gamma_6^-_1\rangle$ (100%)

$\Psi_3$: $0.2814|3.5, \Gamma_8^-_2\rangle$ (8%)+$0.7461|3.5, \Gamma_8^-_3\rangle$ (56%)$-0.6028|3.5, \Gamma_8^-_4\rangle$ (36%)

$\Psi_4$: $-0.9993|3.5, \Gamma_8^-_1\rangle$ (99.9%)

$\Psi_5$: $-0.9082|3.5, \Gamma_8^-_2\rangle$ (82.5%)+$0.4093|3.5, \Gamma_8^-_3\rangle$ (17%)

$\Psi_6$: $-0.308|3.5, \Gamma_8^-_2\rangle$(9.5%) $-$ $0.5242|3.5, \Gamma_8^-_3\rangle$(27.5%) $-$ $0.793|3.5, \Gamma_8^-_4\rangle$ (63%)

$\Psi_7$: $0.9996|3.5, \Gamma_7^-_1\rangle$ (99.9%)

$\Psi_8$: $-0.9996|3.5, \Gamma_7^-_2\rangle$ (99.9%)

$\Psi_9$: $0.9616|2.5, \Gamma_8^-_1\rangle$ (92.5%) + $0.262|2.5, \Gamma_8^-_3\rangle$ (7%)

$\Psi_{10}$: $0.2581|2.5, \Gamma_8^-_1\rangle$ (7%)+$0.3588|2.5, \Gamma_8^-_2\rangle$ (13%) $-$ $0.8933|2.5, \Gamma_8^-_3\rangle$ (80%)

$\Psi_{11}$: $0.3919|2.5, \Gamma_8^-_2\rangle$ (15%) + $0.2076|2.5, \Gamma_8^-_3\rangle$ (4%) $-$ $0.8915|2.5, \Gamma_8^-_4\rangle$ (79.5%)

$\Psi_{12}$: $-0.8451|2.5, \Gamma_8^-_2\rangle$ (71%) $-$ $0.2989|2.5, \Gamma_8^-_3\rangle$ (9%) $-$ $0.4421|2.5, \Gamma_8^-_4\rangle$ (19.5%)

$\Psi_{13}$: $0.9996|2.5, \Gamma_7^-_1\rangle$ (99.9%)

$\Psi_{14}$: $0.9996|2.5, \Gamma_7^-_2\rangle$ (99.9%)

where the point group irreducible representation bases $|J, \Gamma_{m^-_n}\rangle$ are consistency with that of Ref. [23], and $n$ stands for the $n$th component of $\Gamma'_{m^-}$.

According to the absorption, photoluminescence spectra and wavefunctions, the energy level structure of $Yb^{3+}$ in $Ba_2YTaO_6$ can be given, as shown in Fig. 8. Due to time inversion symmetry, $\Psi_1 - \Psi_2$, $\Psi_3 - \Psi_6$, $\Psi_7 - \Psi_8$, $\Psi_9 - \Psi_{12}$, $\Psi_{13} - \Psi_{14}$ degenerate into the same energy levels, which are labeled by $(^2F_{7/2})\Gamma_6^-$, $(^2F_{7/2})\Gamma_8^-$, $(^2F_{7/2})\Gamma_7^-$, $(^2F_{5/2})\Gamma_8^-$ and $(^2F_{5/2})\Gamma_7^-$, respectively. It can be seen that $\Psi_3$, $\Psi_5$, $\Psi_9 - \Psi_{12}$ have the obvious $\Gamma_8^-$ mixing from the multiplets $^2F_{5/2}$ and $^2F_{7/2}$. This situation does not exist in other wavefunctions, whose irreducible representation components account for more than 99% and they can be labeled by the corresponding irreducible representation symbols. The energy level structure of $Yb^{3+}$ in $Ba_2YNbO_6$ can be also obtained with the same way (as shown in Fig. 9).

The transition $(^2F_{7/2})\Gamma_6^- \rightarrow (^2F_{5/2})\Gamma_7^-$ is forbidden by the selection rules of electric and magnetic dipole transitions and can not be observed experimentally.

The odd-order crystal field parameters of $O_h$ are zero, so the electric-pole transition of $Yb^{3+}$ in $Ba_2YTaO_6$ and $Ba_2YNbO_6$ does not exist. The characteristic absorption and emission of $Yb^{3+}$ in $Ba_2YTaO_6$ and $Ba_2YNbO_6$ are from the magnetic pole transition, which usually are much weaker than electric-pole transition. The magnetic-pole transition line strengths of $Yb^{3+}$ in $Ba_2YTaO_6$ and $Ba_2YNbO_6$ from $(^2F_{5/2})\Gamma_8^-$ to the low-energy state were calculated with their wavefunctions in the space spaned by $\{|SLJM\rangle\}$, and were listed in Table 5. The results suggest that the lifetimes of the excite state $(^2F_{5/2})\Gamma_8^-$ are very long, up to milliseconds.

**Table 5.** Line strengths $S_{\rm md}$ from $|^2F_{5/2}, \Gamma_8^-\rangle$.

| | Yb:$Ba_2YTaO_6$ | Yb:$Ba_2YNbO_6$ |
|---|---|---|
| $S_{\rm md}(10^{-20}/{\rm cm}^2)$ | $\lambda$ = 967.29 nm: 0.177 | $\lambda$ = 969.25 nm: 0.177 |
| | $\lambda$ = 1005.23 nm: 0.221 | $\lambda$ = 1006.23 nm: 0.264 |
| | $\lambda$ = 1063.94 nm: 0.291 | $\lambda$ = 1061.92 nm: 0.292 |

## 4. Conclusions

The structures of as-prepared $Yb^{3+}$-doped double-perovskites $Ba_2YB'O_6$ ($B'$= $Ta^{5+}$, $Nb^{5+}$) were refined by Rietveld method, and their structure parameters were calculated. Under the excitation of ultraviolet light, these phosphors show broad charge transfer band emissions of $TaO_6$, $NbO_6$ centres at 390 and 530 nm, which have large Stokes shifts with 12382 and 12979 $cm^{-1}$, respectively. The $Yb^{3+}$ ion in the $Ba_2YB'O_6$ ($B'$= $Ta^{5+}$, $Nb^{5+}$) crystals forming a cubic centre are studied by means of optical spectroscopy. The broad emission bands of $Yb^{3+}$:$Ba_2YB'O_6$ ($B'$= $Ta^{5+}$, $Nb^{5+}$) located at 968, 1005, 1064 nm and 969, 1006, 1062 nm, respectively. The experimental energy levels of $Yb^{3+}$:$Ba_2YB'O_6$ ($B'$= $Ta^{5+}$, $Nb^{5+}$) are determined by diffuse reflection absorption, excitation and emission spectra. The wavefunctions and theoretical energy levels are obtained by diagonalising the Hamiltonian matrix. The experimental energy levels are fitted by Levenberg–Marquardt iteration algorithm to determine crystal field parameters. The Stark splitting of the ground multiplet $^2F_{7/2}$ and the upper multiplet $^2F_{5/2}$ in these

cubic centres, comprise 943 and 904 $cm^{-1}$, 643 and 615 $cm^{-1}$, respectively. The lifetimes of the excite state $(^2F_{5/2})\Gamma_8^-$ are very long, up to milliseconds. It seems that $Yb^{3+}$:$Ba_2YTaO_6$ and $Yb^{3+}$:$Ba_2YNbO_6$ may be good candidates for laser materials.

## References


[1] Kurian J, Nair K V O, Sajith P K, John A M and Koshi J 1998 *Appl. Supercond.* **6** 259

[2] Gröger B, Kulawik J, Szwagierczak D and Skwarek A 2009 *Solid State Ionics* **180** 872

[3] Moreira R L, Abdul Khalam L, Sebastian Mailadil T and Dias A 2007 *J. Eur. Ceram. Soc.* **27** 2803

[4] Sivakumar V and Varadaraju U V 2008 *J. Solid State Chem.* **181** 3344

[5] Yu C C, Liu X M, Yu M, Lin C K, Li C X, Wang H and Lin J 2007 *J. Solid State Chem.* **180** 3058

[6] Falin M L, Gerasimov K I, Leushin A M and Khaidukov N M 2008 *J. Lumin.* **128** 1103

[7] Bespalov V F, Kazakov B N, Leushin A M and Safiullin G M 1997 *Fiz. Tverd. Tela* (St. Petersburg) **39** 1030

[8] Bespalov V F, Kazakov B N, Leushin A M and Safiullin G M 1997 *Fiz. Tverd. Tela* (St. Petersburg) **39** 1532

[9] Saines P J, Spencer J R, Kennedy B J, Kubota Y, Minakata C, Hano H, Kato K and Takata M 2007 *J. Solid State Chem.* **180** 3001

[10] Saines P J, Kennedy B J and Elcombe M M 2007 *J. Solid State Chem.* **180** 401

[11] Rietveld H M 1969 *J. Appl. Cryst.* **2** 65

[12] Larson A C and von Dreele R B 2004 *General Structure Analysis System* (GSAS), Los Alamos National Laboratory Report LAUR **86–748**

[13] Saines P J, Spencer J R, Kennedy B J and Avdeev M 2007 *J. Solid State Chem.* **180** 2991

[14] Eng H W, Barnes P W, Auer B M and Woodward P M 2003 *J. Solid State Chem.* **175** 94

[15] Blass G 1980 *Struct. Bond.* (Heidelberg: Springer-Verlag) **42** 1

[16] Blass G, Dirksen G J, Brixner L H and Crawford M K 1994 *J. Alloys Compd.* **209** 1

[17] van Pieterson L, Heeroma M, de Heer E and Meijerink A 2000 *J. Lumin.* **91** 177

[18] Görller-Walrand C and Binnemans K In: Gschneidner Jr K A and Eyring L (eds) 1996 *Handbook on the Physics and Chemistry of Rare Earths* (Amsterdam, New York, Oxford: North-holland Publishing Company) **23** 250

[19] Li Q Y, Guan Z and Bai F S 2000 *Numerical Computation Principles* (Beijing: Tsinghua University Press) p294

[20] Zhang Q L, Ning K J, Xiao J, Ding L H, Zhou W L, Liu W P, Yin S T and Jiang H H 2010 *Chin. Phys.* **19** 087501

[21] Newman D J and Betty N G 2000 *Crystal Field Handbook* (Cambridge: Cambridge University Press) p162

[22] Koster G F, Dimmock J O, Wheeler R G and Statz H 1963 *Properties of the Thirty-two Point Groups* (Cambridge, Massachusetts: MIT Press) p103

[23] Görller-Walrand G and Binnemans K In: Gschneidner Jr K A and Eyring L (eds) 1996 *Handbook on the Physics and Chemistry of Rare Earths* (Amsterdam, New York, Oxford: North-holland Publishing Company) **23** 182